Article

Electrochemical behavior of copper in simulated concrete pore solutions

Ángel Bacelis[a], Lucien Veleva[a]*, Emmanuel Mena-Morcillo[a] and Mario A. Alpuche-Aviles[b]

[a]Applied Physics Department, Center for Investigation and Advanced Study (CINVESTAV-IPN), Merida Unit, 97310 Merida, Mexico.

[b]Department of Chemistry, University of Nevada, Reno, 1664 N. Virginia St., Reno, Nevada, 89557, USA.

*Correspondence: veleva@cinvestav.mx; Tel.: +521-999- 9429447

Received: date; Accepted: date; Published: date

Abstract: The electrochemical behaviour of copper was studied for 30 days in two model alkaline electrolytes: saturated $Ca(OH)_2$ and cement extract, which were employed to simulate concrete pore environments. The electrochemical tests revealed that sat. $Ca(OH)_2$ is less aggressive to Cu surface, and in consequence, the open circuit potential values of Cu were significantly more positive; also the EIS impedance values were higher in one order of magnitude. The higher value of limiting anodic diffusion current of Cu in cement extract electrolyte also confirmed the aggressivity of this media. Based on the processed current density fluctuations, analyzed as electrochemical noise (EN), the Power Spectral Density (PSD) plots indicated that the initial corrosion attacks on the Cu surface are quasi-uniform, resulting from stationary persistent electrochemical process occurring in both solutions. These results correlated well with the copper surface analysis. XPS analysis and X-ray diffraction patterns revealed that in sat. $Ca(OH)_2$ solution a Cu_2O/CuO corrosion layer was formed on the surface, which effectively protect the metallic Cu, while in cement extract this layer also contains $Cu(OH)_2$. The results suggest that the copper corrosion develops in different ways in each concrete pore model solution, the extract cement electrolyte being more aggressive for copper.We present evidence for the sequential oxidation of Cu to the (+1) and (+2) species and its impact on the corrosion layer and its protecvite properties.

Keywords: copper concrete; cement extract; corrosion; electrochemical noise.

1. Introduction

Concrete embedded metals corrode in fresh and humid concrete where the direct metal oxidation in the pore alkaline environment leads to changes at the metal interface during the curing time. The corrosion process can stop when a protective oxide film is formed on the metal surface, the so-called passive layer. If the concrete is dry, it is unlikely to promote metal corrosion. However, the corrosion could proceed later in the hardened concrete when

its pores, capillaries and cavities contain humidity and dissolved ionic ingredients extracted from the cement that are aggressive against metal, in the presence of oxygen diffused at the metal surface. Further, this internal electrolyte increases the electrical conductivity of concrete, which increases the rates of electrochemical processes that in turn accelerate the corrosion process.

According to Halstead's report [1], copper pipes are used in concrete when there is no contamination with ammonia. Metals other than reinforcing steel frequently embedded in or used in contact with concrete are principally aluminum, copper, lead, and zinc [2].

According to Pourbaix diagrams [3], copper may have good corrosion resistivity in neutral aqueous salt solutions in a wide pH range, as well as it is relatively not sensitive to chloride salts, because of the slight solubility of copper(I)-chloride corrosion product. It is reported that in air a Cu(I)-oxide layer forms on copper and its alloys, which once embedded in most concrete or cement mortar, undergoes negligible uniform corrosion because this layer presents slight solubility [4, 5]. In cement with higher alkalinity (pH value of the cement stone pores solution > 13.3), copper is not sufficiently resistant. According to the Portland Cement Association, copper surface should be protected when it comes into contact with concrete mixtures containing high sulfur components, such as ash and fly ash, because they may lower the pH, and promote a relatively acidic environment that is highly corrosive to most metals, including copper [6].

The corrosion of copper has been examined in alkaline aqueous solutions. For example, in borax solutions with pH 9.2 [7] and pH 9.7 [8], the formation of a passive multilayer of copper oxides and hydroxides occurs on the metal surface. In borate buffer-mix solution of 0.3 M H_3BO_3 and 0.075 M $Na_2B_4O_7$ (1: 4) with pH 8.4, the results of the cyclic voltammetry suggest the passivation of copper and the formation of a film of $Cu_2O/CuO\text{-}Cu(OH)_2$ duplex oxide, the internal layer of Cu_2O of which acts as protective barrier and the outer layer is formed by $CuO\text{-}Cu(OH)_2$ hydrate complex [9]. The corrosion behavior of copper was investigated in aqueous solutions of different pH values, using electrochemical and surface analysis methods [10].

The electrochemical semi-reactions involved in copper corrosion in alkaline media are [11]:

Anodic reaction:

$$Cu \rightarrow Cu^{2+} + 2e^-, \quad (1)$$

Cathodic reaction:

$$O_2 + H_2O + 4e^- \rightarrow 4OH^-, \quad (2)$$

At pH 10, a thin compact film of Cu_2O is formed on the surface and spontaneously passivated Cu. The general reaction of the formation of Cu_2O at slightly alkaline pH [11] is shown by the following equation:

$$2Cu + 2OH^- \rightarrow Cu_2O + H_2O + 2e^-, \quad (3)$$

At sufficiently high pH (12 to 13 pH values) the Cu surface is covered mainly with a protective monoclinic cupric oxide (CuO) layer and the general reaction of its direct formation is [11]:

$$Cu + 2OH^- \rightarrow CuO + H_2O + 2e^-, \quad (4)$$

Another important reaction in this type of alkaline environment is the formation of copper hydroxide ($Cu(OH)_2$)[11]:

$$Cu + 2OH^- \rightarrow Cu(OH)_2 + 2e^-, \quad (5)$$

Impedance measurements [8, 9] suggest that the corrosion process has been controlled by the oxygen diffusion process through the oxide layer. Summing up the reported results, it may be stated that the main products of copper corrosion in alkaline media are Cu_2O, CuO and $Cu(OH)_2$.

Studies of corrosion embedded metals corrosion is a topic of discussion with regards to instrumental techniques and data interpretation [12, 13]. Difficulties in experimental measurements include the electrode and cell design, the potential drop (IR) in the concrete and its compensation, the development of macro-corrosion cells and the restriction of oxygen diffusion, to mention a few. The use of submerged electrodes in model solutions that simulate the concrete pore electrolyte avoids many of the above difficulties [14-16]. The model solutions allow comparative results to be obtained and control of some testing parameters, which are difficult to achieve in concrete samples, mainly not homogeneous in their internal surface. Many model solutions have been proposed, including the use of a saturated aqueous solution of $Ca(OH)_2$ (pH 12-13) [12, 16-20], aqueous KOH and NaOH [21-24], and cement extract solution [25, 26]. The most commonly reported model is the saturated $Ca(OH)_2$ solution. However, the composition of the concrete pore solution is more complex [26], since it includes other compounds extracted from the cement in the presence of humidity, in addition to $Ca(OH)_2$. Previously, several studies have reported the electrochemical corrosion behavior of carbon steel, stainless AISI 304 and 316 in pore model solutions [14, 27-33].

Despite the use of copper in the construction industry, very little systematic work has been carried out on the behavior of copper and its alloys in contact with concrete, and their corrosion mechanism in concrete pore solutions has not yet been clarified. Therefore, in view of the advantages of model solutions it is appropriate to study the corrosion behavior of copper in this type of environment, because it allows to obtain comparative results and to control some testing parameters which are difficult to achieve in not homogeneous internal surface of concrete samples. In structural engineering, the contact of metal and mineral materials, which are produced with cement, plays an important role from a corrosion-technical point of view. There are few studies on the corrosion susceptibility of copper

exposed to concrete environments, and most of which do not employ electrochemical techniques even though they have the advantage of being practical and fast [34].

In this work, we characterize the initial stages of electrochemical corrosion of copper exposed to two model electrolyte solutions for up to 720 h (30 days), simulating the electrolyte of the concrete pore, viz saturated calcium hydroxide solution and cement extract solution, (renamed as I and II solutions, respectively). The research was carried out with different electrochemical and surface analysis methods, such as eclectrochemical impedance spectroscopy (EIS), potentiodynamic polarization (PDP) curves, cyclic voltammetry (CV) and electrochemical noise (EN) of current fluctuations, scanning electron microscopy (SEM) and X-Ray Diffraction (XRD). Some authors have used some of these techniques to characterize the attack suffered by steels in concrete [35, 36] or in solutions that simulate concrete [37], as well as to determine the corrosion products that are formed during this process.

2. Materials and Methods

2.1. Samples and solution preparation

Copper sheet (> 99.99 %) was cut into square samples of 1 cm^2. All samples were abraded with wet SiC paper, sonicated, and dried in air prior to immersion tests. The solution I, used to simulate the non-carbonated concrete pore, was prepared from analytical grade reagent $Ca(OH)_2$ (Sigma-Aldrich, St. Louis, MO, USA) and ultrapure deionized water (18.2 MΩ•cm). For the solution II a 1:1 wt./wt. mixture of Portland cement type I was used and ultrapure deionized water. Table 1 gives the chemical composition of the cement used and that of solution II. The mixture was stored for 24 h in order to allow cement hydration, and it was kept in a sealed container to avoid absorption of CO_2 from the air. Subsequently, the suspended particles were removed from the supernatant by filtering the solution II with a 125 mm pore-size filter paper (Whatman, Kent, UK). Copper behavior was studied in the absence of chlorides, because the copper surface in concrete is not usually exposed to Cl^- ions during the initial stages. The pH values of the solutions I and II were 12 and 13 respectively. The pH was regularly checked by a pH meter and the Cu samples were immediately immersed, to avoid carbonation effects.

Table 1. Composition of cement according to the producer and chemical analysis of the cement extract solution.

Compound	Weight %	Cement solution
SiO_2	21.35	-
Al_2O_3	4.87	as Al^{3+}
Fe_2O_3	2.89	as Fe^{3+}
CaO	66.84	as Ca^{2+}
K_2O	0.39	-
Na_2O	0.08	-
SO_3	2.42	-
MgO	1.16	as Mg^{2+}

140

141 *2.2. Immersion tests and surface characterization*

142 The Cu flat samples (1x1x0.3 cm) were exposed to solutions I and II according to the ASTM
143 standard guide for laboratory immersion corrosion testing of metals [38]. They were
144 withdrawn after 360 and 720 hours, rinsed with deionized water, and dried in air at room
145 temperature (21ºC). In order to evaluate the damage on the copper surface, the corrosion
146 products formed were removed from the surface through the cleaning procedure
147 recommended by ASTM G1 standard [39]. Further, their surfaces were characterized by
148 Scanning Electron Microscopy (SEM-EDS, XL-30 ESEM-JEOL JSM-7600F). The corrosion
149 products were analyzed with X-Ray Diffraction instrument (Siemens D-5000) and X-Ray
150 Photoelectron Spectroscopy (K-Alpha, Thermo Scientific).

151 *2.3. Electrochemical measurements*

152 An Interface-1000E potentiostat/galvanostat/ZRA (Gamry Instruments, Philadelphia, PA,
153 USA) was used for electrochemical experiments, with a typical three-electrode cell
154 configuration inside a Faraday cage. The working electrode was the copper plate with an
155 exposed area of 0.8 cm^2, Pt plate was used as auxiliary and a saturated calomel electrode
156 (SCE) as reference electrode. All experiments were carried out at room temperature (21 ºC).
157 Electrochemical Impedance Spectroscopy (EIS) measurements were performed at the open
158 circuit potential (OCP), applying an AC signal of ± 15 mV amplitude, in a frequency range
159 from 100 kHz to 10 mHz, and with a sampling size of 10 data points/decade. EIS diagrams
160 were recorded at different immersion periods in solutions I and II: 30 minutes (initial), 24 h,
161 360 h and 720 h. Potentiodynamic polarization (PDP) curves were made for comparative
162 purposes at initial time of immersion (30 minutes), with a scan rate of 10 mV s^{-1}, starting
163 from -0.5 V to 0.5 V vs OCP. Both EIS diagrams and PDP curves were analyzed with Gamry
164 Echem Analyst ® software (Gamry Instruments). Cyclic Voltammetry was carried with scan
165 rate of 25 mV s^{-1}. Before voltammetry experiments, the open circuit potential of the

electrodes in the model solution was monitored until it stabilized (30 min). All CV scans started in open circuit potential and them carrying in cathodic direction. For each sample, 10 cycles were run, which had a similar behavior, so the 5th cycle was chosen in each case. All potentials are referred to the SCE, and anodic currents are shown as positive.

For Electrochemical Noise measurements (EN), two identical working electrodes and the SCE reference electrode were employed, according to ASTM G199-09 standard [40]. The three electrodes were connected to the potentiostat in the zero-resistance ammeter mode (ZRA) to record both current and potential values with a sampling frequency of 1 Hz during 24 h. Subsequently, the acquired EN signals were preprocessed, transformed and analyzed by the Electrochemical Signal Analyzer ® software (Gamry Instruments).

3. Results

Copper plates were prepared in the same manner as those exposed were used as control. Figure 1 shows the surface of the copper sample as well as its elemental analysis using EDS, this shows high copper content corresponding to the matrix, as well as a smaller oxygen content.

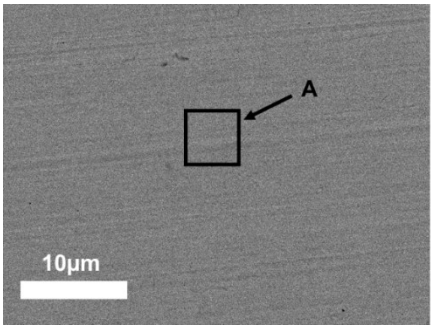

	A
Element	Weight %
Cu	99.58
O	0.42

Figure 1. SEM images (3000x) and EDS analysis of the copper without exposing.

Figure 2 shows the XPS of a control Cu sample exposed to air, without immersing it in solution. The XPS determined the existence of a native copper oxide layer on the polished surface of the copper without exposure to solution. Because it was not possible to detect it by XRD (see below) it follows that it is probably due to a thin or amorphous layer. Despite the low oxygen content presented in the EDS analysis for the control sample, XPS analysis (Fig. 2) mainly indicates presence of Cu_2O which seems to form immediately on the surface of the copper when it comes in contact with the atmosphere.

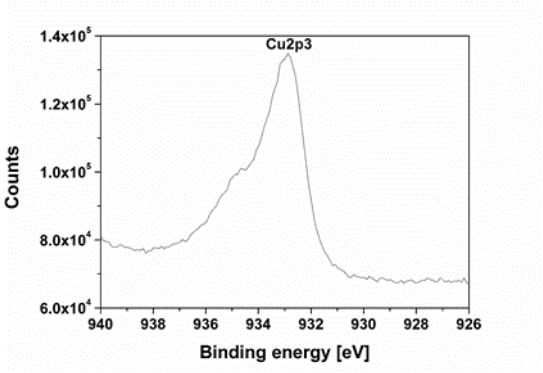

Figure 2. Cu 2p3/2 spectra for Cu.

3.1. Surface morphology and analysis of the Cu surface after exposure to solutions I and II

3.1.1Scanning Electronic Microscopy

SEM images and EDS analysis of Cu surface after exposure for 360 h and 720 h to solution I are shown in Figure 3 (a-b). Two different morphological zones are visible in the formed layers: the lighter A, the darker B. The layer characteristic of zone A presents high contents of copper and relatively low of oxygen, which ratio probably corresponds to copper oxide and the copper surface attacked. EDS analysis indicates the presence of Ca traces in zone A, while in zone B calcium content is significant, accompanied by higher oxygen and carbon contents. These results permit the conclusion that the layer in the darker zones B could be considered as formed by $CaCO_3$; the main product of the reaction of atmospheric CO_2 with $Ca(OH)_2$ [41], even though the container was open only during the time of measurements.

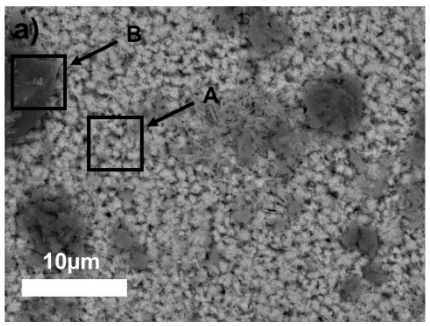

	A	B
Element	Weight %	
Cu	66.88	10.53
O	28.37	56.23
Ca	1.55	18.77
C	3.20	14.47

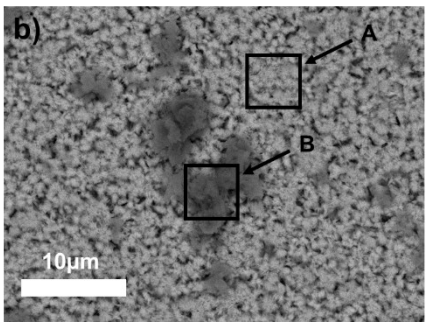

	A	B
Element	Weight %	
Cu	70.82	26.52
O	26.00	43.04
Ca	1.10	17.55
C	2.08	12.89

Figure 3. SEM images (3000x) and EDS analysis of Cu surface after exposure to solution I for 360 h (a) and 720 h (b).

The copper surface also changes after immersion in solution II for 360 (Fig. 4a) and 720 hours (Fig. 4b), presenting formed layers having a morphology and elemental composition of two distinguishable zones labeled as A and B. The EDS composition of zones A is very similar to that observed on copper after exposure to solution I for 360 and 720 h (Fig. 3a-b), indicating that the surface is mainly covered by Cu-oxide. Meanwhile, in the small zones, B over time, the formation of $CaCO_3$ (Fig. 4 b) prevails, as more significant in content than that of Cu-oxide. At the later period of 720 h of exposure in solution I (Fig. 1b), the Cu surface mainly changed its morphology, presenting crystals with larger size in the zones A and B. The EDS analysis also shows the presence of elements such as Na, K, and Al probably from solution II.

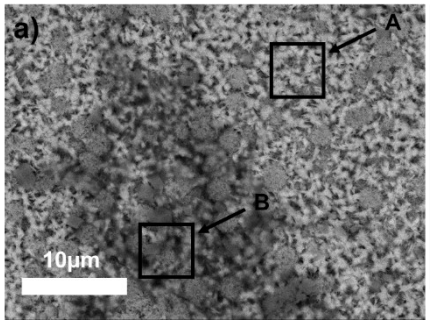

	A	B
Element	Weight %	
Cu	67.95	34.57
O	27.37	28.16
Ca	1.31	2.35
C	2.60	27.98
Na	-	4.06
K	0.77	2.88

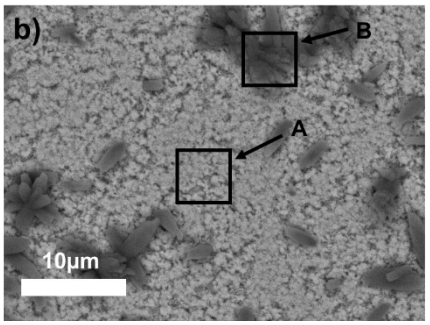

	A	B
Element	Weight %	
Cu	69.68	13.80
O	27.72	51.29
Ca	0.45	19.41
C	1.84	15.49
Al	0.32	-

Figure 4. SEM images (3000x) and EDS analysis of Cu surface after exposure to solution II for 360 h (a) and 720 h (b).

Figure 5 compares Cu surfaces, the corrosion layers of which were removed after exposure for 720 h to solution I (Fig. 5 a), and solution II (Fig. 5 b). The images indicate that the observed corrosion attack on the copper surface occurs similarly in both model solutions.

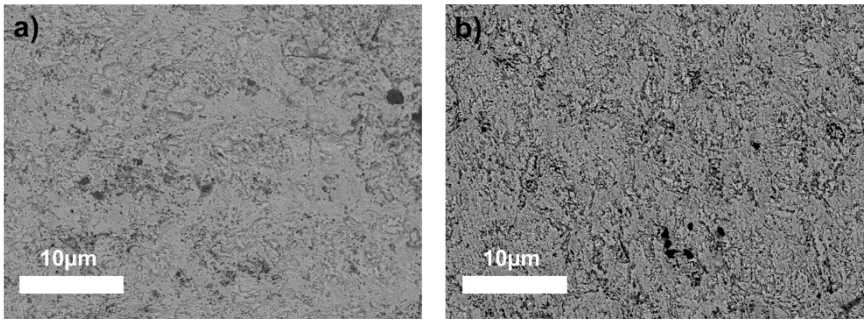

Figure 5. SEM images (x3000) of Cu surfaces, after removing of corrosion layers formed during exposure to both model solutions for 720 h: a) solution I and b) solution II.

Figure 6 shows the cross-section of the corrosion layers formed after 720 h of exposure in each model solution. It can be seen that the surface attack on the surface of Cu is similar in both solutions, which was developed in form of cavities. It can also be seen that the layer of corrosion products is thin (about a few microns) for both cases. .

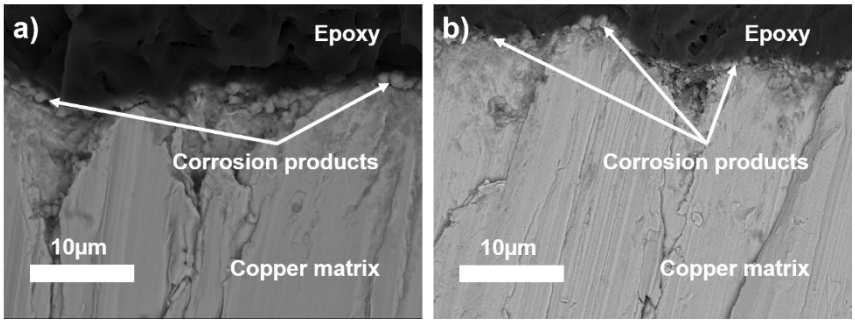

Figure 6. SEM images of copper samples cross-section (x3000), a) solution I and b) solution II.

3.1.2. X-ray diffraction patterns

According to the reports [7-10] in alkaline solution the corrosion layer consists of *tenorite* (CuO), *cuprite* (Cu_2O), as two stable oxides having black and reddish color, respectively, and copper hydroxide ($Cu(OH)_2$). Figure 7 presents X-ray diffraction patterns of the layers formed on Cu surface after exposure for 360 and 720 hours in each model solutions. It can be seen that CuO was formed as a corrosion product, accompanied by $CaCO_3$ at very low intensity on the samples immersed in solution I for 360 h and 720 h (Fig. 7a-c). At the later stage (720 h) in this solution also appear low signal of Cu_2O, another corrosion product.

In the case of samples immersed in solution II for both times (Fig. 7b-d) CuO was detected as in solution I, as well as $CaCO_3$. However, $Cu(OH)_2$ also was detected for both stages, and this fact suggests that in solution II a layer of CuO and $Cu(OH)_2$ is formed on the surface.

In our previously reported work AISI 316 corrosion behavior was compared in the same model solutions [14, 32]. Based on optical microscope and AFM images, as well as XPS and electrochemical tests, we recommended the use of cement extract solution as simulated concrete pore environment, because it represents a variety of ions as part of the cement.

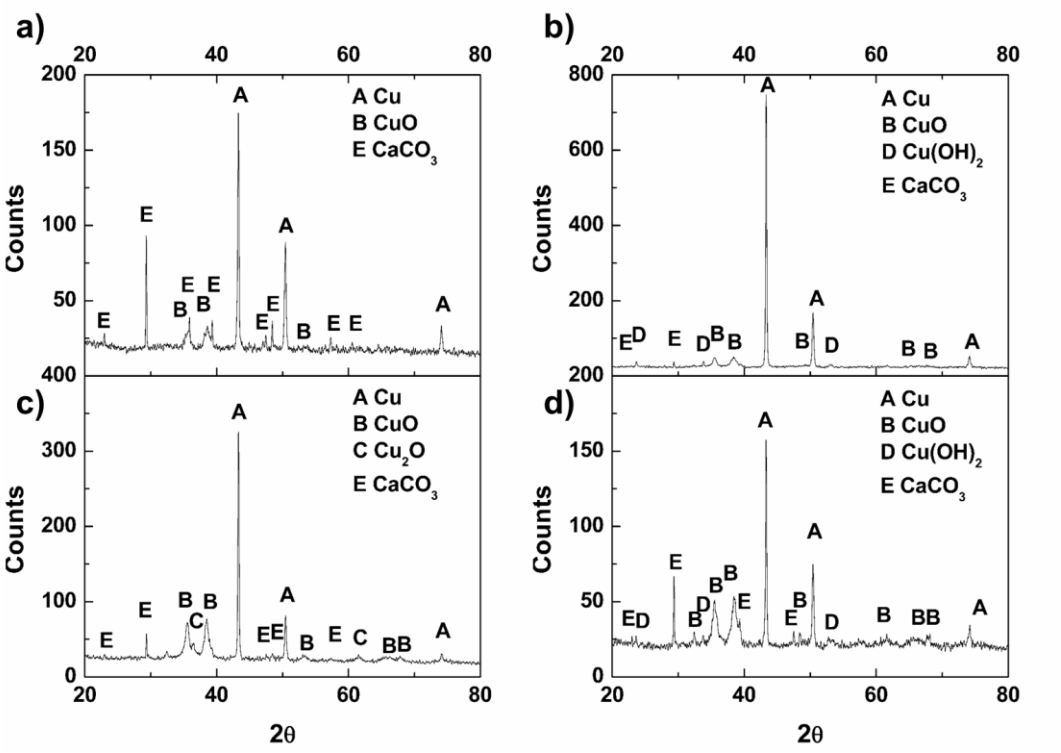

Figure 7. X-ray diffraction patterns comparing the crystalline compounds formed on Cu surface after 360 hours of exposure to: a) solution I and b) solution II, and after 720 hours of exposure to: c) solution I and d) solution II.

3.1.3. X-ray Photoelectron Spectroscopy

XPS analysis was used to determine the formation of corrosion products on the copper surface during the first hours of exposure in both solutions, XRD patterns just detect metallic copper due to the thickness of the oxides formed during these times. XPS analysis of the surface of the samples exposed to solution I for 1 h and 24 h (Fig. 8a-b) also indicates the presence of Cu_2O in both cases, this can be attributed to the fact that in the first hours of exposure in this solution, the patina formed in the absence of electrolytes is a thin layer on the surface.

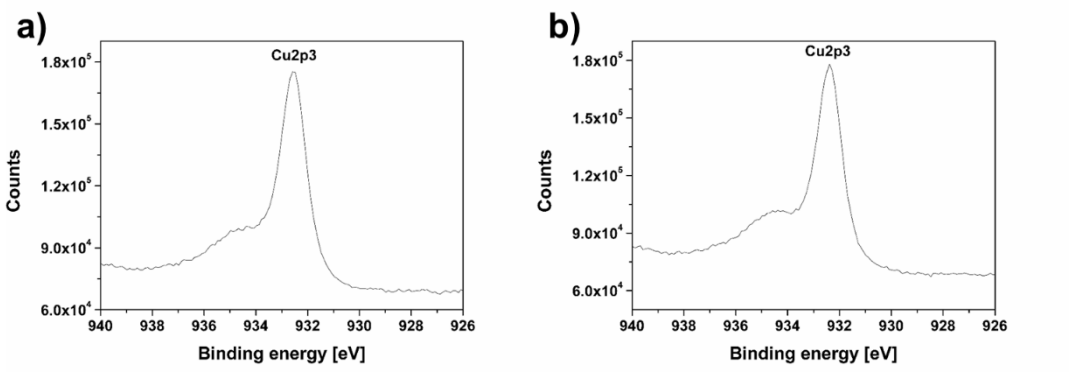

Figure 8. Cu 2p3/2 spectra for Cu exposure to solution I: a) 1 h and, b) 24 h.

On the other hand, the XPS analysis of the sample exposed in solution II during the first hour (Fig. 9a) shows a behavior like those exposed to solution I, that is, Cu_2O remains on the surface. However, at longer times in this solution (Fig. 9b) in addition to the formation of Cu_2O, the XPS analysis indicates the presence of CuO.

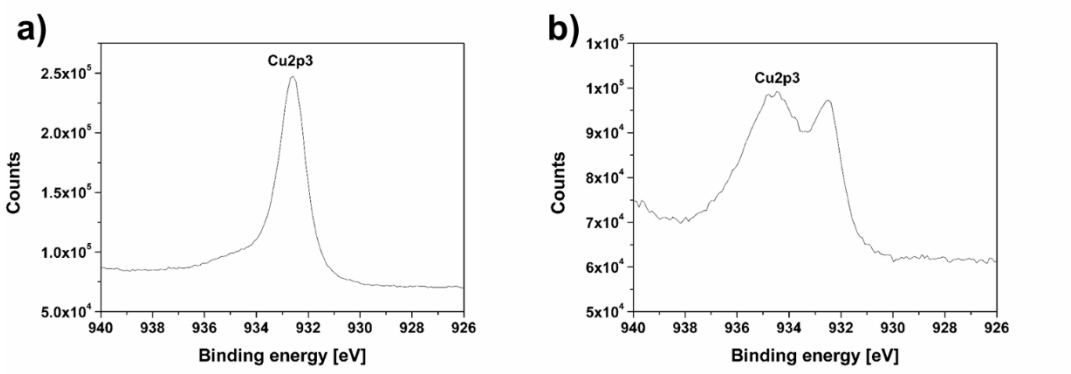

Figure 9. Cu 2p3/2 spectra for Cu exposure to solution II: a) 1 h, and, b) 24 h.

3.2. Electrochemical measurements

3.2.1. Open circuit potential (o.c.p)

Table 2 shows the recorded values of free corrosion potential (o.c.p.) of Cu exposed for different immersion times in each model medium: solutions I and II. It should be noted that the initial value of o.c.p. of Cu in solution I is more positive than that of copper in solution II. In addition, it moves with ≈123 mV to a more positive value at the end of this experiment (Table 2), indicating the growth of a protective layer from the immersion, that of CuO according to the XRD spectra (Fig. 7c). However, Cu o.c.p. in solution II, each time it was experienced, there were less positive values, compared to those recorded in solution I (Table 2). Up to 360 h o.c.p. measured in solution II showed a very slight trend towards a more positive value at ≈30 mV probably due to the formation of CuO or $Cu(OH)_2$ as indicated by XPS and DRX, followed by a return to a less value positive at ≈50 mV. Probably due to the arrival of O to the bare metal, after passing through the product layer indicating that the corrosion product layer formed in solution II is less protective.

Table 2. Change in time of open circuit potential values of Cu exposed to I and I solutions.

Time (h)	**Solution I mV vs SHE**	**Solution II mV vs SHE**
Initial	62 ± 0.07	47 ± 0.12
24	108 ± 0.01	81 ± 0.33
360	136 ± 0.02	79 ± 0.05
720	152 ± 0.07	29± 0.04

3.2.2. Electrochemical Impedance Spectroscopy (EIS)

Figure 10 presents EIS Nyquist plots for a copper surface, exposed for different times (up to 720 h) to each model solutions. The depressed semicircle shape can be attributed to the double-layer capacitance, as well as to the charge transfer resistance of the surface, because of the layers formed on it. In the case of copper in solution I (Fig.10a) it may be seen that the size of the depressed semicircle increases with time, up to the maximum exposure time of 720 h. However, in solution II (Fig. 10b) the depressed arch increases up to 360 h of immersion and then follows a slight decay, probably due to the arrival of O through the product layer, as mentioned above. The difference in the protective efficiency of the layers grown on copper reflects the order of the impedance magnitude, i.e. one order lower in solution II, indicating that the corrosion layer is less protective for the copper surface that that formed in solution II. This fact correlates well with the more positive values of o.c.p. in model solution I, reported above (Table 2).

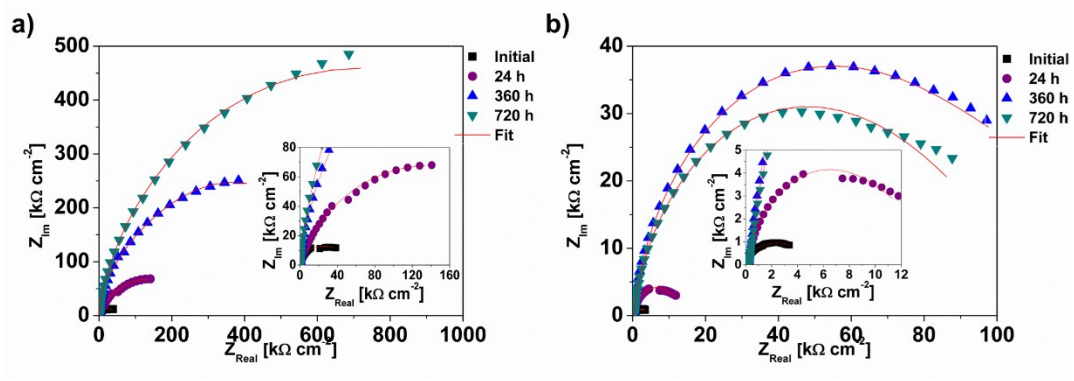

Figure 10. EIS Nyquist plots for a copper exposed up to 30 days (720 h) to two model concrete pore solutions: a) solution I and b) solution II.

At high frequencies (between 100 and 1000 Hz), the EIS Bode plots (Fig. 11) show the total impedance associated with the solution resistance (R_{sol}) at the Cu-electrolyte interface and specifics of the electrochemical corrosion process. There is approximately one order of difference in R_{sol}, being higher in solution I, which fact indicates that the CuO film is difficult for penetration of active species and oxygen molecules. At frequencies between 1 Hz and 0.01 Hz, the total impedance can be attributed to the electrochemical corrosion process, which occurs on the metal surface (formation of corrosion products – Cu_2O, CuO, $Cu(OH)_2$) [42-44]. It may be seen that as time passes, the tendencies in change of the total impedance for copper in both solutions follow those reported above for o.c.p. values (Table 2). The EIS diagrams suggest also that the copper behavior followed different mechanism in I and II concrete pore model solutions.

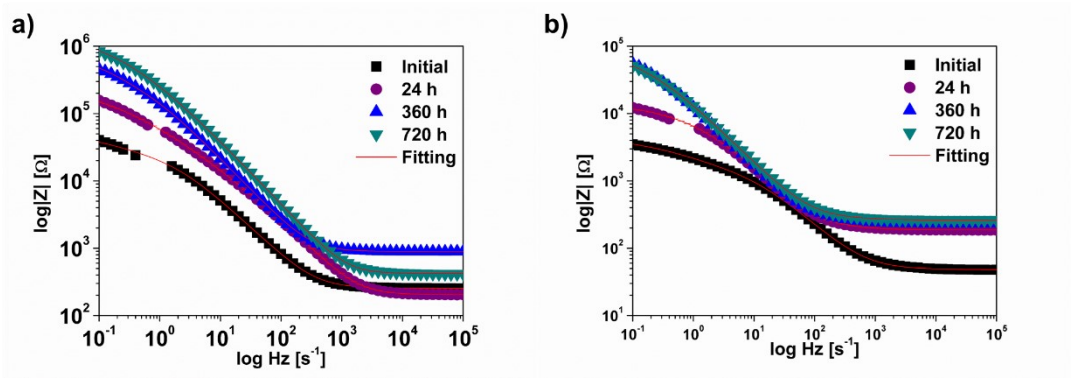

Figure 11. EIS Bode plots for a copper exposed up to 30 days (720 h) in: a) solution I and b) solution II.

The equivalent electric circuit that theoretically models the behavior of copper exposed to each model solutions is presented in Figure 12.This circuit has adequately fit the experimental data (adequacy < $5x10^{-4}$ for the experimental data modeled mathematically obtained with the circuit).

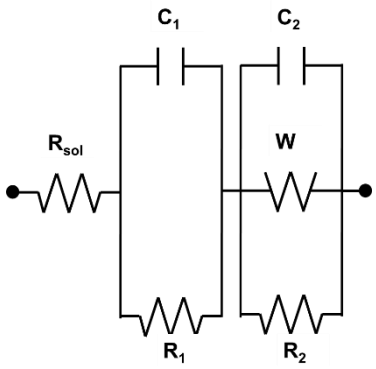

Figure 12. Equivalent electric circuit fitted to the EIS plots of copper exposed to I and II model solutions.

The circuit as proposed includes a capacitor (C_1) and a resistor (R_1), both associated with the external corrosion product layer (CuO or CuO-$Cu(OH)_2$). The internal layer (Cu_2O) is characterized by a capacitor (C_2), a resistor (R_2) and a Warburg impedance element (W). The Warburg impedance in lower frequencies indicates that the corrosion process is also controlled by the diffusion of ionic species and molecules (such as O_2, participating in the cathodic reaction) through the layers of products formed on the copper surface [18, 45, 46]. For satisfactory EIS diagram simulation, it is necessary to replace the capacitors (C_1 and C_2) with a constant phase element (CPE) in the equivalent circuit [47]. The most accepted common explanation for the presence of CPE and depressed semicircles on solid electrodes is the microscopic roughness, causing a non-inhomogeneous distribution in the solution resistance, as well as in the double-layer capacitance [48].

330 3.2.3. Potentiodynamic polarization curves

331 Figure 13 presents the potentiodynamic polarization curves of copper, exposed to each
332 model solution. It should be noted that both cathodic curves display very close values,
333 indicating that the cathodic process occurs in a similar way. Furthermore, they do not present
334 Taffel region, corresponding to activation control on the cathodic process (oxygen
335 reduction), and the diffusion-limited current is reached after the first -50 mV of initial
336 polarization (vs o.c.p.), when the diffusion of oxygen consumed at the cathodic sites is
337 controlling the cathodic process. A similar fact has been reported for copper sheet in alkaline
338 media [49].

339 The anodic curves registered on Cu surface exposed to each model solution do not present
340 the Tafel region either, and the corrosion process is controlled by the diffusion transport. It
341 may be observed that the diffusion-limited current starts at approximately +30 mV of initial
342 polarization (vs o.c.p.) and continues up to ≈+100 mV, where the formation of corrosion layer
343 probably begins, as was suggested by XPS and XRD spectra. However, it should be noted
344 that the value of the diffusion-limited current of Cu exposed to solution II is one order higher
345 than that in solution I, which confirms that this solution (II) is more aggressive for Cu surface.
346 These results correlate well with EIS spectra (Fig.6) and o.c.p. values (Table 2), again
347 permitting the conclusion that both electrolytes, which model concrete pore solution, present
348 different aggressivity.

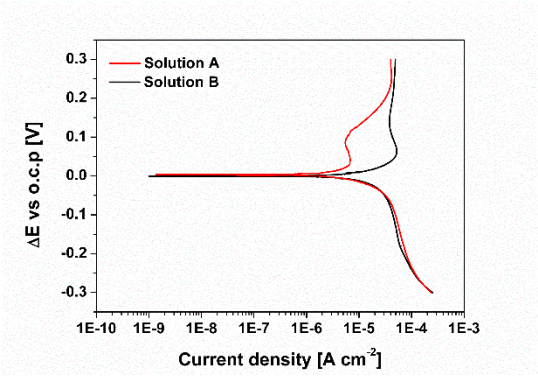

349

350 **Figure 13.** Potentiodynamic polarization curves of Cu exposed to two concrete pore model
351 electrolytes: solution I, saturated $Ca(OH)_2$ (red curves) and solution II, cement extract (black
352 curves).

353 3.2.4. Electrochemical noise measurements

354 The fluctuations of Cu-electrode current density, exposed to each model electrolytes, were
355 reordered at open circuit potential after the first 24 h (Fig. 14). The amplitude of the
356 fluctuations was about 3 μA cm^{-2} and they were considered as electrochemical noise (EN),
357 which indicates a quasi-stationary, persistent process in this initial period occurring on the
358 Cu surface. The EN signals (Fig.14) were processed with the software, giving the values of
359 σ_i and i_{rms} corresponding to the standard deviation and the mean square root of the current

noise, respectively. They were used to calculate the pitting index (PI), to reveal the susceptibility of copper surface to uniform or localized corrosion in these initial stages up to 24 hours, following the proposed equation [50]:

$$PI = \sigma_i \, (i_{rms})^{-1}, \quad (5)$$

The values of $PI_{Sol.\ I}$ = 0.180 and $PI_{Sol.\ II}$ = 0.116 indicated that in both concrete pore media there are quasi-uniform attacks on the copper surface. According to the ASTM standard [40], only PI values above 0.6 may indicate localized corrosion. The obtained PI values correlate with the low amplitude of the current fluctuations, which are characteristic of the uniform corrosion process [51].

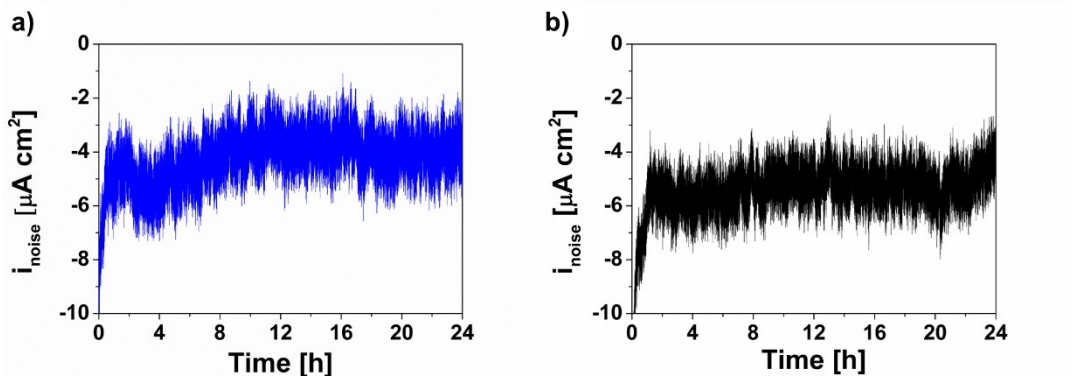

Figure 14. Current density signals recorded during 24 h of exposure of Cu to a) solution I and b) solution II.

Figure 15 shows the Power Spectral Density (PSD) graph of the preprocessed current density signals (from Fig. 14), and its corresponding slope (*β*), also known as the spectral power exponent: 0.90 in solution I and 0.94 in solution II. According to fractal analysis, this *β* value is related to the process of fractional Gaussian noise (*fGn*, -1 <β <+1) [52-54]. The *fGn* is a property representative of self-similarity and persistent stationary processes, as suggested by Eke et al. [52]. The persistence measures the correlations between adjacent values within a time series, while the stationary aspect reflects that all moments are independent of the length of the time series [55]. The latter could be related to the persistent process of breakdown in the copper naturally formed oxide film of Cu_2O, which in contact with both alkaline media will proceed to a the nucleation of a CuO and $Cu(OH)_2$ corrosion product later, as it was suggested by the XRD spectra (Fig.7).

Thus, the EN results lead to the conclusion that the quasi-uniform corrosion of Cu surface in both model solutions in the first 24 h of immersion was a stationary persistent process.

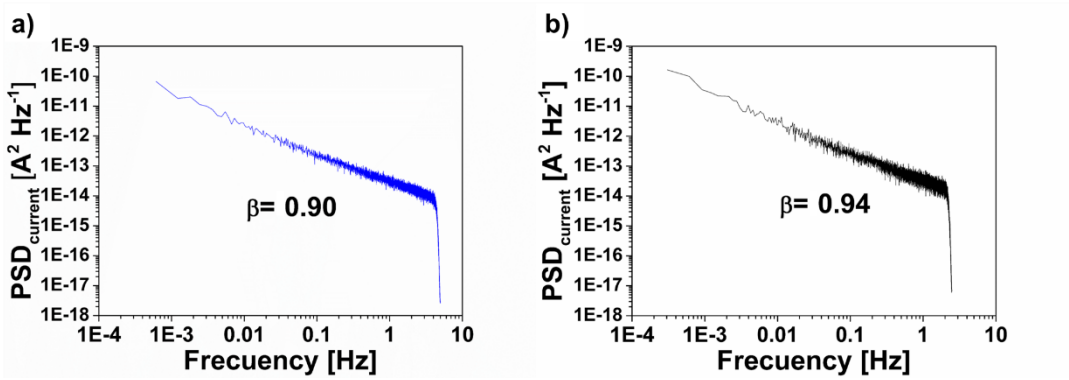

Figure 15. PSD plots of EN current signals from Figure 14 and the obtained *β* values for Cu exposed to: a) solution I and b) solution II.

3.2.5. Cyclic voltammetry measurements

Figure 16 shows the voltammograms of the exposed copper in I and II solutions. Voltammograms show two peaks in the anodic region. The first peak (A) is attributed to the oxidation of metallic copper to cuprous oxide (Cu_2O) and the second (B) to CuO or $Cu(OH)_2$ [56-58], although thermodynamically the CuO is more stable [59].

Two possible reaction pathways for the formation of Cu_2O (peak A) have been proposed, the direct oxidation of copper, via a one electron step that lead to the formation of Cu_2O (Ec. 6) [11] which initially leads to Cu(OH) , which again breaks down into Cu_2O through the following reactions [56]:

$$Cu + OH^- \rightarrow Cu(OH) + e^-, \quad (6)$$

$$2Cu(OH) \rightarrow Cu_2O + H_2O, \quad (7)$$

However, reaction (3) is thermodynamically more likely [60]:

$$2Cu + 2OH^- \rightarrow Cu_2O + H_2O + 2e^-, \quad (3, \text{restated})$$

because the Cu^+, and thus, Cu(OH) are not stable species.

The second peak (B) is probably due to the oxidation of cuprous oxide to either (or both) CuO and $Cu(OH)_2$ according to the following equations [56]:

$$Cu_2O + 2OH^- \rightarrow 2CuO + H_2O + 2e^- \quad (8)$$

$$Cu_2O + 2OH^- + H_2O \rightarrow 2Cu(OH)_2 + 2e^- \quad (9)$$

The resulting $Cu(OH)_2$ exists in the following equilibrium for solution II [57]:

$$Cu(OH)_2 \rightarrow CuO + H_2O \quad (10)$$

Therefore, it is assumed that the second peak of the anodic region could be a multilayer CuO film in contrast to the Cu_2O monolayer under the first peak [57].

In the cathodic region, there are peaks C and D that are attributed to the reduction of Cu_2O, CuO and $Cu(OH)_2$ [60]. Peak C could be attributed mainly to the reduction of CuO or Cu(OH)2 to Cu_2O. On the other hand, peak D could be attributed to the reduction of the Cu_2O to metallic Cu [56-57,59-60].

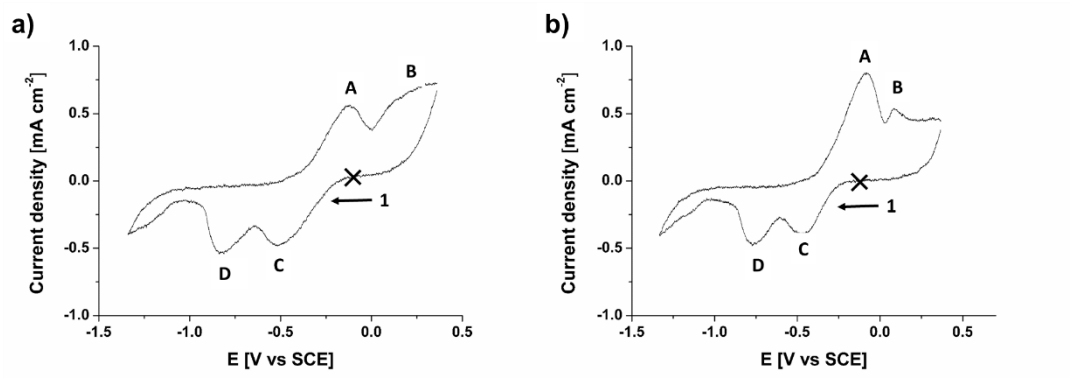

Figure 16. Cyclic voltammograms of Cu at the initial time in a) solution I and b) solution II.

The CVs the sample exposed to solution I (Fig. 16a) has a lower current density in the peak A (anodic region) compared to the sample exposed to solution II (Fig. 12b), indicating that the oxide layer (Cu_2O) that forms in the copper surface exposed to solution I has better protection.

On the other hand, Figure 17 shows the change in the anodic and cathodic peaks when 25 mV s^{-1} and 100 mV s^{-1} scan rates are used. It can be seen that with the exception of peak D (reduction of Cu_2O to metallic Cu), no other peak (A, B, C) behaves according to $i\ \alpha\ v^{1/2}$. This indicates that these processes are not completely controlled by diffusion.

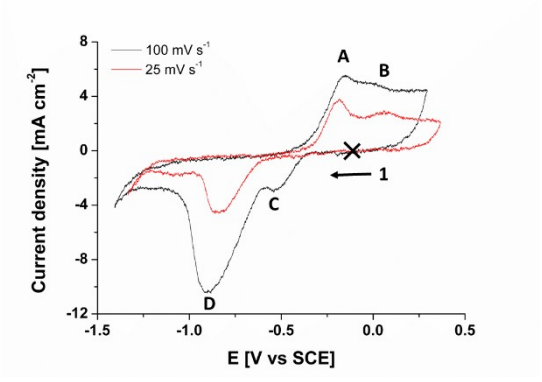

Figure 17. Cyclic voltammograms of Cu in solution II at sweep rate 25 mV (red line) and 100 mV (black line).

4. Conclusions

The present work compares the electrochemical behavior of copper exposed to saturated calcium hydroxide and cement extract alkaline solutions up to 720 h (30 days), as two model

electrolytes simulating the concrete pore. The electrochemical tests revealed that in solution II, cement extract, the corrosion layer includes several ions in addition to Ca^{2+}. With time, the composition of the corrosion layer changes in a manner different from those of the corrosion layer formed in solution I, saturated $Ca(OH)_2$. As a consequence, the open circuit potential values of Cu are significantly less positive in solution II, cement extract, and the EIS impedance magnitude are in one order lower, indicating that the formed layer is less protective for the copper surface than that formed in solution I. The equivalent electric circuit obtained for EIS, which models the behavior of copper, fitted satisfactorily to the Nyquist plots. Additionally, we note that the value of the limiting anodic diffusion current of Cu exposed to solution II is one order of magnitude higher than that in solution I, confirming that solution II, cement extract, is more aggressive for the Cu surface. The current density fluctuations of Cu electrodes, considered as electrochemical noise (EN) their Power Spectral Density (PSD), indicate that the initial corrosion attacks on the Cu surface could be considered as quasi-uniform, in accordance with the calculated pitting index (PI), resulting from persistent stationary electrochemical process on the copper surface in both model concrete pore media. These results correlate well with the surface analysis corresponding to copper surfaces exposed to both model solutions for different periods of time. XPS analysis showed that on both surfaces initially, there is a *cuprite* (Cu_2O) layer and this layer remains for 24 h in both solutions. X-ray diffraction patterns revealed that in solution I, *tenorite* (CuO) is the predominant corrosion product on the copper surface, while in II, cement extract, this layer also contains $Cu(OH)_2$. Overall, our results lead to the conclusion that although there are similarities like the fact that model solutions attack the surface in a quasi-uniform manner, the overall copper corrosion develops in different ways in each concrete pore model solution. The extract cement electrolyte is more aggressive towards the copper surface. In the CV experiments, anodic peaks correspond to the formation of a Cu_2O monolayer, followed by a complex layer of CuO or $Cu(OH)_2$ under potentiodynamic conditions consistent with the sequential formation of Cu^{1+} and Cu^{2+} and therefore, we consider that the corrosion mechanism occurs via two, one-electron oxidation steps.

Author Contributions:

Á.B. performed the preparation of samples and their corrosion tests. E.M.M contributed to the methodology and technical preparation of the results. M.A.A.A. contributed to the methodology and technical interpretation of the results. Á.B. and L.V. discussed the results and wrote the manuscript, with contributions of all authors. L.V. supervised the project. All correspondence should be addressed to L.V.

Funding: M.Sci. Ángel Adrián Bacelis Jiménez and M. Sci. Emmanuel Mena Morcillo extend warm thanks to CONACYT, awarding their scholarship as Ph.D. students at CINVESTAV-IPN, Applied Physics Department. Further, the authors express their gratitude to LANNBIO-

CINVESTAV for permitting the use of their facilities, as well as Dora A. Huerta-Quintanilla, Daniel Aguilar and Wilian Cauich for their technical assistance in SEM-EDS, XRD, and XPS analysis. MAA acknowledges support of NSF Career Award CHE-1255387 and MRI-1726897.

References

1. Halstead, P.E., *The corrosion of metals in contact with concrete.* Chem. & Ind, 1957. **34**: p. 1132-1137.
2. Woods, H., *Corrosion of Embedded Materials Other Than Reinforcing Steel*, in *Significance of Tests and Properties of Concrete and Concrete-Making Materials*. 1966, ASTM International.
3. Pourbaix, M., *Atlas of Electrochemical Equilibria in Aqueous Solution.* NACE, 1974. **307**.
4. Nürnberger, U., *Korrosion und Korrosionsschutz im Bauwesen, Band 1 Grundlagen.* Betonbau, Bauverlag GmbH, Wiesbaden, Berlin, 1995.
5. BAUSTOFFEN, M. and D. MATERIAUX, *Corrosion of metals in contact with mineral building materials.* Otto-Graf-Journal, 2001. **12**: p. 69.
6. Freedman, S., *Corrosion of nonferrous metals in contact with concrete.* Modern Concrete, 1970. **36**.
7. Strehblow, H.-H. and B. Titze, *The investigation of the passive behaviour of copper in weakly acid and alkaline solutions and the examination of the passive film by ESCA and ISS.* Electrochimica Acta, 1980. **25**(6): p. 839-850.
8. Ribotta, S., L. Gassa, and M. Folquer, *Characterization of anodic films formed on copper in 0.1 M borax solution.* Journal of Electroanalytical Chemistry, 2008. **624**(1-2): p. 262-268.
9. Babić, R., M. Metikoš-Huković, and A. Jukić, *A study of copper passivity by electrochemical impedance spectroscopy.* Journal of the Electrochemical Society, 2001. **148**(4): p. B146-B151.
10. Feng, Y., et al., *Corrosion mechanisms and products of copper in aqueous solutions at various pH values.* Corrosion, 1997. **53**(5): p. 389-398.
11. King, F., *Corrosion of copper in alkaline chloride environments*. 2002, Swedish Nuclear Fuel and Waste Management Co.
12. Francis, P., *The use of synthetic environments for corrosion testing*. 1988: ASTM International.
13. Berke, N.S. and V. Chaker, *Corrosion rates of steel in concrete*. 1990: ASTM International.
14. Veleva, L., et al., *Comparative cyclic voltammetry and surface analysis of passive films grown on stainless steel 316 in concrete pore model solutions.* Journal of Electroanalytical Chemistry, 2002. **537**(1-2): p. 85-93.
15. Cabrini, M., et al., *Effect of Organic Inhibitors on Chloride Corrosion of Steel Rebars in Alkaline Pore Solution*. Vol. 2015. 2015. 1-10.
16. Cabrini, M., S. Lorenzi, and T. Pastore, *Cyclic voltammetry evaluation of inhibitors for localised corrosion in alkaline solutions.* Electrochimica Acta, 2014. **124**: p. 156-164.

17. Andrade, C., et al., *Cement paste hardening process studied by impedance spectroscopy.* Electrochimica acta, 1999. **44**(24): p. 4313-4318.
18. Jiang, J.-y., et al., *Pitting Corrosion Behaviour of New Corrosion-Resistant Reinforcement Bars in Chloride-Containing Concrete Pore Solution.* Materials, 2017. **10**(8): p. 903.
19. Jiang, J.-y., et al., *The Passive Film Growth Mechanism of New Corrosion-Resistant Steel Rebar in Simulated Concrete Pore Solution: Nanometer Structure and Electrochemical Study.* Materials, 2017. **10**(4): p. 412.
20. Cabrini, M., S. Lorenzi, and T. Pastore, *Study of localized corrosion of steel reinforcement in inhibited alkaline solutions [Studio della corrosione localizzata degli acciai per armature in soluzioni alcaline inibite]*. Vol. 105. 2013. 21-31.
21. Oranowska, H. and Z. Szklarska-Smialowska, *An electrochemical and ellipsometric investigation of surface films grown on iron in saturated calcium hydroxide solutions with or without chloride ions.* Corrosion Science, 1981. **21**(11): p. 735-747.
22. Berman, H., *The Effect of Sodium Chloride on the Corrosion of Concrete Reinforcing Steel and on the pH of Calcium Hydroxide Solution*. 1974.
23. Ftikos, C. and G. Parissakis, *The combined action of Mg2+ and Cl− ions in cement pastes.* Cement and Concrete Research, 1985. **15**(4): p. 593-599.
24. Zakroczymski, T., C. Fan, and Z. Szklarska-Smialowska, *Kinetics and Mechanism of Passive Film Formation on Iron in 0.05 M Sodium Hydroxide.* Journal of Electrochemical Society, 1985. **132**: p. 2,862.
25. Montemor, M. and A. Simoes, *Analytical Characterization of the Passive Film Formed on Steel in Cement Past Intersticial Solutions.* PORTUGALIAE ELECTROCHIMICA ACTA, 1995. **13**: p. 453-456.
26. Montemor, M., A. Simoes, and M. Ferreira, *Analytical characterization of the passive film formed on steel in solutions simulating the concrete interstitial electrolyte.* Corrosion, 1998. **54**(5): p. 347-353.
27. Moreno, M., et al., *Corrosion of reinforcing steel in simulated concrete pore solutions: effect of carbonation and chloride content.* Corrosion Science, 2004. **46**(11): p. 2681-2699.
28. Saremi, M. and E. Mahallati, *A study on chloride-induced depassivation of mild steel in simulated concrete pore solution.* Cement and Concrete Research, 2002. **32**(12): p. 1915-1921.
29. Bertolini, L., et al., *Behaviour of stainless steel in simulated concrete pore solution.* British corrosion journal, 1996. **31**(3): p. 218-222.
30. Chen, W., et al., *Study on the corrosion behavior of reinforcing steel in simulated concrete pore solutions using in situ Raman spectroscopy assisted by electrochemical techniques.* Electrochimica Acta, 2010. **55**(20): p. 5677-5682.
31. Zhang, F., J. Pan, and C. Lin, *Localized corrosion behaviour of reinforcement steel in simulated concrete pore solution.* Corrosion Science, 2009. **51**(9): p. 2130-2138.
32. Veleva, L., et al., *Voltammetry and surface analysis of AISI 316 stainless steel in chloride-containing simulated concrete pore environment.* Journal of Electroanalytical Chemistry, 2005. **578**(1): p. 45-53.
33. Fajardo, S., et al., *Low-nickel stainless steel passive film in simulated concrete pore solution: A SIMS study.* Applied surface science, 2010. **256**(21): p. 6139-6143.

34. Duffó, G.S., S.B. Farina, and F.M.S. Rodríguez, *Corrosion behaviour of non-ferrous metals embedded in mortar.* Construction and Building Materials, 2019. **210**: p. 548-554.
35. Bragança, M.O., et al., *Performance of Portland cement concretes with 1% nano-Fe3O4 addition: Electrochemical stability under chloride and sulfate environments.* Construction and Building Materials, 2016. **117**: p. 152-162.
36. Andrade, C., et al., *Electrochemical behaviour of steel rebars in concrete: influence of environmental factors and cement chemistry.* Electrochimica Acta, 2001. **46**(24-25): p. 3905-3912.
37. Freire, L., et al., *Electrochemical and analytical investigation of passive films formed on stainless steels in alkaline media.* Cement and Concrete Composites, 2012. **34**(9): p. 1075-1081.
38. *Standard Guide for Laboratory Immersion Corrosion Testing of Metals*.
39. *Standard Practice for Preparing, Cleaning, and Evaluating Corrosion Test Specimens*. 2017.
40. *Standard Guide for Electrochemical Noise Measurement*. 2014, ASTM International: West Conshohocken, PA.
41. Fernández, J. and M. Renedo, *Sulfation and Carbonation Competition in the Treatment of Flue Gas from a Coal-Based Power Plant by Calcium Hydroxide.* International Journal of Chemical Reactor Engineering, 2015. **13**(2): p. 177-182.
42. Yasuda, H., Q. Yu, and M. Chen, *Interfacial factors in corrosion protection: an EIS study of model systems.* Progress in organic Coatings, 2001. **41**(4): p. 273-279.
43. Xia, S., et al., *Electrochemical studies of AC/DC anodized Mg alloy in NaCl solution.* Journal of The Electrochemical Society, 2004. **151**(3): p. B179-B187.
44. Wen, L., et al., *Microstructure and corrosion resistance of modified 2024 Al alloy using surface mechanical attrition treatment combined with microarc oxidation process.* Corrosion Science, 2011. **53**(1): p. 473-480.
45. Nikfahm, A., et al., *Effect of grain size changes on corrosion behavior of copper produced by accumulative roll bonding process.* Materials Research, 2013. **16**(6): p. 1379-1386.
46. Pan, C., et al., *Atmospheric Corrosion of Copper Exposed in a Simulated Coastal-Industrial Atmosphere.* Journal of materials science & technology, 2017. **33**(6): p. 587-595.
47. Danaee, I., M.N. Khomami, and A. Attar, *Corrosion behavior of AISI 4130 steel alloy in ethylene glycol–water mixture in presence of molybdate.* Materials Chemistry and Physics, 2012. **135**(2-3): p. 658-667.
48. Danaee, I. and S. Noori, *Kinetics of the hydrogen evolution reaction on NiMn graphite modified electrode.* international journal of hydrogen energy, 2011. **36**(19): p. 12102-12111.
49. Yeganeh, M. and M. Saremi, *A comparison between the corrosion behavior of nanostructured copper thin films deposited on oxidized silicon and copper sheet in alkaline media.* Surface and Coatings Technology, 2010. **205**(7): p. 2218-2224.
50. Kearns, J.R., et al., *Electrochemical noise measurement for corrosion applications*. Vol. 1277. 1996: ASTM International.
51. Legat, A. and V. Dolecek, *Corrosion monitoring system based on measurement and analysis of electrochemical noise.* Corrosion, 1995. **51**(4): p. 295-300.
52. Eke, A., et al., *Physiological time series: distinguishing fractal noises from motions.* Pflügers Archiv, 2000. **439**(4): p. 403-415.

53. Delignieres, D., et al., *Fractal analyses for 'short'time series: a re-assessment of classical methods.* Journal of mathematical psychology, 2006. **50**(6): p. 525-544.
54. Malamud, B.D. and D.L. Turcotte, *Self-affine time series: measures of weak and strong persistence.* Journal of statistical planning and inference, 1999. **80**(1-2): p. 173-196.
55. Liu, X., H. Wang, and H. Gu, *Fractal characteristic analysis of electrochemical noise with wavelet transform.* Corrosion science, 2006. **48**(6): p. 1337-1367.
56. Zaafarany, I. and H. Boller, *Electrochemical behavior of copper electrode in sodium hydroxide solutions.* Current World Environment, 2009. **4**(2): p. 277.
57. El Haleem, S.A. and B.G. Ateya, *Cyclic voltammetry of copper in sodium hydroxide solutions.* Journal of Electroanalytical Chemistry and Interfacial Electrochemistry, 1981. **117**(2): p. 309-319.
58. Dong, S., Y. Xie, and G. Cheng, *Cyclic voltammetric and spectroelectrochemical studies of copper in alkaline solution.* Electrochimica acta, 1992. **37**(1): p. 17-22.
59. Latimer, W.M., *Oxidation Potentials Prentice-Hall.* Inc. Englewood Cliffs. NJ, 1952.
60. Ambrose, J., R. Barradas, and D. Shoesmith, *Investigations of copper in aqueous alkaline solutions by cyclic voltammetry.* Journal of Electroanalytical Chemistry and Interfacial Electrochemistry, 1973. **47**(1): p. 47-64.